Propagation dynamics of deformed 2D vortex Airy beams

Yingkang Chen (陈颖康)[1], Xiwen Lin (林茜文)[1], Shuyu Lin (林书玉)[1], Shaoying Mo (莫少莹)[1], Lingyu Wan (万玲玉)[1], and Yi Liang (梁 毅)[1,2,*]

[1]*Guangxi Key Laboratory for Relativistic Astrophysics, School of Physics Science and Technology, Guangxi University, Nanning 530004, China*

[2]*The MOE Key Laboratory of Weak-Light Nonlinear Photonics, TEDA Applied Physics Institute and School of Physics, Nankai University, Tianjin 300457, China*

**Corresponding author: liangyi@gxu.edu.cn*

Received December 25, 2016; accepted April 28, 2017; posted online May 15, 2017

We numerically and experimentally investigate the propagation of deformed 2D vortex Airy beams. Our results show that, for different topological charges, two parabolic trajectories that can be controlled by changing the initial wing angle always dominate the beam propagations. In this case, the main lobes take different propagation distances to restore to the peak intensity. The profiles tend to evolve into 1D or 2D Airy-like patterns to various degrees in the same propagation distance. Furthermore, the whole profiles yield a small change in their acceleration direction, depending on the topological charge and the initial wing angle.

OCIS codes: 080.4865, 080.7343, 050.1940.
doi: 10.3788/COL201715.080801.

Due to their intriguing properties including self-acceleration, non-diffraction, and self-healing[1–3], Airy beams have attracted a lot of attention and inspired tremendous potential applications in manipulation, biophotonics, and communication fields such as manipulation of particles[4,5], generation of curved plasma channels[6], light bullets[7], guiding discharges[8], routing surface plasmons[9–12], electron Airy beams[13], three-dimensional super-resolution imaging[14], light-sheet microscopy[15], and image signal transmission[16]. All of these applications are based on the unique propagation properties of Airy beams. To control the propagation of Airy beams, a lot of work has been done to synthesize various kinds of families of Airy beams. For example, synthesized by three Airy functions, a three-Airy beam linearly diffracts into a super-Gaussian-like beam[17]. A vortex Airy beam can be generated[18] if a spiral phase is imposed. Actually, many works about vortex Airy beams have been done, including their Wigner representation[19], propagation[20], dynamic control of collapse[21], spiral spectrum[22], beam wander[23], chirped Airy vortex beams[24], and so on. All of these vortex Airy beams have 90° angles between their two wings. One question arises: how do vortex Airy beams propagate when their two wing angles do not equal 90°?.

Recently, the dynamics of deformed 2D Airy beams whose wing angles are not 90° were investigated, and it was shown that two acceleration trajectories exist and the profiles change with the angle[25]. Based on this, here, we report a numerical and experimental study on the propagation of deformed 2D Airy beams carrying a phase singularity, i.e., optical vortices (OVs). It is found that, at the same angle between the two wings, this new kind of Airy beams called deformed 2D vortex Airy beams still accelerate along two similar trajectories as the deformed 2D Airy beams. In other words, the self-acceleration of deformed 2D vortex Airy beams is also a result of the "hyperbolic umbilic" catastrophe (a two-layer caustic)[26]. The main lobes will still propagate along a parabolic trajectory, whereas a different path exists to lead to energy flow. Moreover, our results show that, for different topological charges and different angles between two wings of deformed 2D vortex Airy beams, the profiles of the beams exhibit different self-acceleration behavior. First, after a certain propagation distance, these beams tend to evolve into 1D or 2D Airy-like patterns to various degrees. Second, as a result of the orbital angular momentum that the OV possesses, the whole profile of a deformed 2D vortex Airy beam exhibits a small left-hand transversal deflection, while the normal deformed 2D Airy beams always accelerate along the $-y$ direction, as we designed initially. In other words, a deformed 2D vortex Airy beam no longer always accelerates along one direction. Its self-acceleration direction has a small shift. To further explain the above phenomena, the beam feature and the propagation dynamics are also further elaborated by numerically analyzing the internal transverse power flow of the beams. Our theoretical analysis is in good agreement with the associated numerical observations, as well as is demonstrated by experiments.

Theoretically, to simplify our discussion, following the approach previously developed[25], a deformed 2D vortex Airy beam with arbitrary angle θ between its two wings can be designed to accelerate along the $-y$ direction at $z = 0$ as

$$\begin{aligned}\psi(x, y, z = 0) &= \mathrm{Ai}(s_1)\mathrm{Ai}(s_2)\exp(\alpha s_1 + \alpha s_2) \\ &\quad \times [(s_1 - s_{1d}) + \mathrm{i}(s_2 - s_{2d})]^m, \\ s_n &= (-1)^{n-1}\cos\left(\frac{\theta}{2}\right)x/r_0 - \sin\left(\frac{\theta}{2}\right)y/r_0, \quad n = 1, 2, \end{aligned} \tag{1}$$

where Ai( ) is the Airy function, α is determined by the effective aperture of an optical system, s_n represents a dimensionless transverse coordinate, r_0 is an arbitrary transverse scale; s_{1d} and s_{2d} denote the dislocation of the OV from the origin along s_1 and s_2 orientations, respectively; and m is the topological charge of the OV. Using the field described by Eq. (1) as the input, we can calculate the evolution of a deformed 2D vortex Airy beam by solving numerically the paraxial wave equation in free space by the split-step beam propagation method using

$$2ik\partial_z\psi + \partial_{xx}^2\psi + \partial_{yy}^2\psi = 0, \tag{2}$$

where $k = 2\pi n/\lambda$ (n is the refractive index, λ is the wavelength of the beam) is the wavenumber.

Typically, $\alpha = 0.02$, $r_0 = 40$ μm, $s_{1d} = 0$, $s_{2d} = 0$, $n = 1$, and $\lambda = 532$ nm are adopted in this work. When $m = 0$, the propagations of normal deformed 2D Airy beams with different initial angles θ can be obtained based on Eq. (2), as presented in Fig. 1. As mentioned in Ref. [25] and shown in Figs. 1(a4)–1(c4), due to a "hyperbolic umbilic" catastrophe (a two-layer caustic), when $\theta \neq 90°$, i.e., the initial angle between two wings of the beam is an acute angle [Fig. 1(a)] or an obtuse angle [Fig. 1(c)], the propagations of the beams are described by two different parabolic trajectories: one is for the peak intensity of these 2D Airy beams (Y_{d1}: the white dashed curves in Fig. 1), the other is for the main lobes of the 2D Airy beams (Y_{d2}: the green dashed curves in Fig. 1). For the normal 90° case, the peak intensity always stays on the main lobe and they will propagate in a same path [Fig. 1(b)]. Following the analysis presented in Ref. [25], the above two trajectories for the deformed 2D Airy beam are a result of the "hyperbolic umbilic" catastrophe and can be extracted via the catastrophe theory in the paraxial approximation[25,26]:

$$Y_{d1} = \frac{[1-3\sin^2(\theta/2)]\cos^2(\theta/2)}{\sin(\theta/2)} \frac{\lambda^2}{4\pi^2 r_0^3} z^2, \tag{3a}$$

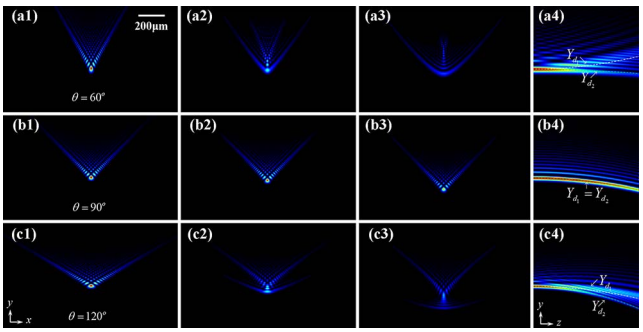

Fig. 1. (Numerical simulations, color online) The propagation of normal deformed 2D Airy beams ($\alpha = 0.02$, $r_0 = 40$ μm, $s_{1d} = 0$, $s_{2d} = 0$, $m = 0$) with different initial angles θ: (a) $\theta = 60°$, (b) $\theta = 90°$, (c) $\theta = 120°$. From the 1st to the 3rd column are the beam profiles at $z = 0$, 4, and 8 cm, respectively, and the last column shows side views of beam propagation up to 8 cm, where the white (Y_{d1}) and green (Y_{d2}) dashed curves are plotted by calculating Eqs. (3a) and (3b), respectively.

$$Y_{d2} = -\frac{\lambda^2 \sin^3\left(\frac{\theta}{2}\right)}{4\pi^2 r_0^3} z^2. \tag{3b}$$

Equation (3a) describes the tendency of the peak intensity associated with the beams and Eq. (3b) depicts the trajectory of the main lobe of the 2D Airy beams. Apparently, both trajectories can be readily controlled with ease by varying the initial wing angle θ and the accelerations of the main lobe increase as θ gets larger, as demonstrated as in Figs. 1(a4)–1(c4).

Furthermore, the catastrophe theory also tells us that these beams will tend to evolve into the well-known 1D or 2D Airy patterns after a certain propagation distance, as described in Ref. [25] (Fig. 1 also presents this phenomenon). 2D Airy beams with $\theta \neq 90°$ could not preserve their pattern as well as the 90° case in linear propagation. The beam shape for $\theta = 60°$ will tend to evolve into a 1D Airy-like pattern [Figs. 1(a1)–1(a3)] while most energy of the beam for an obtuse angle, i.e., $\theta = 120°$ shrinks into a typical 2D Airy-like shape (some power is involved to evolve into a 1D Airy-like pattern) [Figs. 1(c1)–1(c3)].

In this work, our main goal is to study the behavior of vortex Airy beams in detail. So, similar to the investigation of normal deformed 2D Airy beams, when $m = 1$, i.e., the deformed 2D Airy beams with different angles carry an OV with a unit topological charge, the numerical results about propagation of the beams can also be simulated from Eq. (2), as shown as in Fig. 2. In Fig. 2, one can clearly see that the intensity distributions of the beams are changed a lot. Actually, Eq. (2) shows that not only the phase but also the amplitude of the beams is modulated. Moreover, here, we let $s_{1d} = 0$ and $s_{2d} = 0$, viz., the spiral phase superimposes completely on the main lobe of the beams. Therefore, the sidelobes of the beams at the input ($z = 0$ cm) are much stronger than the main lobe. A half-doughnut main lobe replaces the solid main lobe of vortex-free Airy beams ($m = 0$) [the insets in Figs. 2(a1)–2(c1)]. As the propagation distance increases, due to the self-healing property the main lobe will be reconstructed as a solid lobe, i.e., after a certain propagation distance, the main lobe can recover to the peak intensity and continue accelerating along the parabolic

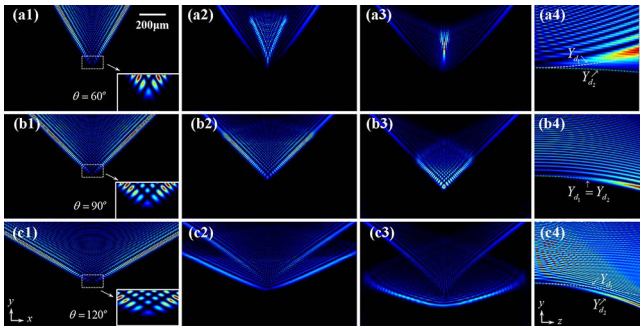

Fig. 2. (Numerical simulations, color online) Same as in Fig. 1 but with a vortex of a unit topological charge ($m = 1$) imposed as in Eq. (1).

trajectory [Y_{d2} plotted as a green dashed curve in Figs. 2(a4)–2(c4)]. It should be noted that the reconstruction distance is related to the initial wing angle. For example, the main lobe of the 90° case reappears at a longer z position than the 120° case [Figs. 2(b4)–2(c4)]. For $\theta = 60°$, the main lobe could not be seen because it needs a longer propagation distance to self-heal [Fig. 2(a)].

Similar to the case of $m = 0$, these beams tend to evolve into the well-known 1D or 2D Airy patterns after a certain propagation distance. However, in this case, for an obtuse angle, i.e., $\theta = 120°$, most of the beam energy spreads into a 1D Airy-like pattern while less energy shrinks into a 2D Airy-like shape. Counter to that, for $\theta = 60°$, most of the beam propagates along the Y_{d1} trajectory [plotted as a white dashed curve in Fig. 2(a4)] and it cannot evolve into a full 1D Airy-like pattern. In Figs. 2(a4)–2(c4), one can also see that the propagation of the beams is still described by two different parabolic trajectories, as in Fig. 1. Thus, one can infer that the propagation dynamics of deformed 2D vortex Airy beams also originates from a "hyperbolic umbilic" catastrophe (a two-layer caustic).

Interestingly, as a result of the orbital angular momentum of OVs, the whole profiles in Fig. 2 will exhibit a very small left-hand deflection when the propagation distance increases, as shown as in Figs. 2(a3)–2(c3). In other words, the acceleration of a deformed 2D vortex Airy beam is not only along the $-y$ direction, but also has a small component along the $-x$ direction. Its acceleration direction has a small shift. Specifically, this left-hand deflection of the profile enhances while θ gets larger. That is because the null energy distribution of the beams is governed by the Airy function and the OV cannot exceed the main lobes of the beams. So, the vortex structure will always be limited by the main lobe and the left-hand deflection gets larger when the acceleration of the main lobe goes up with the wing angle θ.

Keeping all of the conditions the same as in Figs. 1 and 2, we also study the deformed 2D vortex Airy beams when $m = 2$. Comparing with the intensity distributions of Figs. 1 and 2, it is seen that for $\theta = 60°$ we observe hardly any energy extending into a 1D Airy-like shape while most of the energy of the beam for $\theta = 120°$ evolves into 1D Airy-like pattern, as depicted in Figs. 3(a) and 3(c). Moreover, comparing with the 2D vortex Airy beams carrying a unit spiral phase, the whole intensity profiles in Fig. 3 exhibit a bigger left-hand deflection at the same propagation distance due to a bigger orbital angular momentum density of OVs for $m = 2$. Apparently, as introduced by the same reason as in Fig. 2, the left-hand deflections of the main lobes in Fig. 3 are enhanced when the initial wing angle θ gets larger. In Figs. 3(a4)–3(c4), the two parabolic trajectories Y_{d1} and Y_{d2} expressed by Eq. (3) still limit the acceleration of the beams along the same path, as in the case of $m = 0, 1$. However, comparing with the case of $m = 0, 1$, the main lobes of these beams almost disappear and need a longer distance to restore to the peak intensity.

In order to get a more intuitive explanation of the beam dynamics, the above phenomena that resemble self-healing in Figs. 1–3 can be better examined by analyzing the internal transverse power flow associated with the 2D Airy beams[3,25]. Figure 4 shows the transverse power flow of the 2D Airy beams with $\theta = 60°, 90°, 120°$ numerically calculated at different topological charges. When $m = 0$, most of the whole transverse power flow is along the direction of $-y$ [Fig. 4(a)]. For $\theta < 90°$, the power of the main lobe flows outward, toward the sidelobes [Fig. 4(a1)]. Thus, the acceleration of the main lobe along the $-y$ direction is reduced. Meanwhile, the two wings expand when their power flows outward in the horizontal direction. As a result, a part of the beam evolves into a 1D Airy-like shape. In contrast, for $\theta > 90°$, the power of the sidelobes flows toward the main lobe [Fig. 4(a3)].

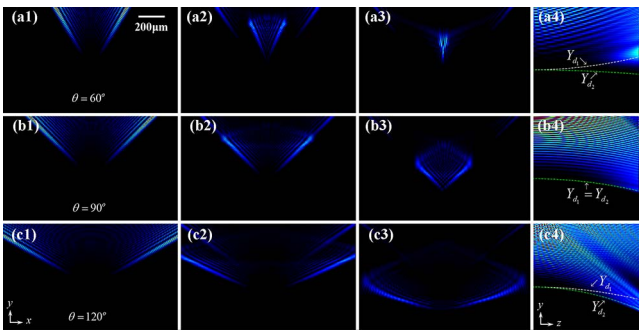

Fig. 3. (Numerical simulations, color online) Same as in Fig. 1 but with a vortex of two unit topological charges ($m = 2$) imposed as in Eq. (1).

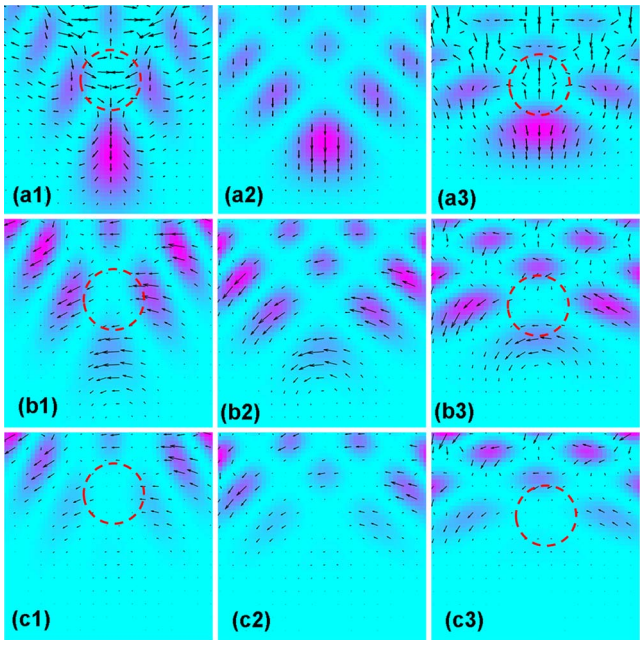

Fig. 4. (Color online) Transverse power flow of the 2D Airy beams carrying different topological charges at $z = 0.3$ mm: (a) $m = 0$, (b) $m = 1$, (c) $m = 2$. From the 1st to the 3rd column corresponds to different initial wing angles: $\theta = 60°$, $\theta = 90°$, and $\theta = 120°$, respectively.

This inward flow enhances the acceleration of the main lobe along $-y$ while it leads to the elongation of the main lobe and turns it into a 1D Airy-like pattern [Fig. 1(c)]. In addition, as mentioned in Ref. [25], in the region marked by the red circles in Figs. 4(a1) and 4(a3), the overall influx of the power is larger than the outflow, which indicates the shifting of the peak intensity from the main lobe to the sub lobes and causes two different acceleration paths. Moreover, this power flow will evolve into a 2D Airy-like shape, which is more obvious for >90°.

When $m = 1, 2$, one can see that the transverse power flow of the beams is along an anticlockwise rotation direction, which implies that a left-hand deflection will happen on the whole intensity distribution. Moreover, compared with the case of $m = 0$, there is less and less power to flow into the areas marked by the red dashed circles. In other words, it is not easy to transfer part of the power to a 2D Airy-like shape while more and more power from the sidelobes expands outward as a 1D Airy-like shape [Figs. 2(c3) and 3(c3)]. Furthermore, for a larger initial angle and the same topological charge, the anticlockwise-rotation power flow is along a bigger orbital radius [Figs. 4(b1)–4(b3)]. Clearly, the 2D beams with a larger initial angle possess orbital angular momentum density and a larger transversal shift on the acceleration direction. It should be emphasized that, for $m = 2$, there are weak anticlockwise-rotation power flows existing because of the bigger modulation on amplitude and leads to a weaker transverse power flow. Actually, according to the property of OVs, the orbital angular momentum density is bigger with a bigger topological charge. Thus, for $m = 2$, the beams will still exhibit a larger deflection in the acceleration direction.

In order to verify the above analysis, we performed a series of experiments to investigate the propagation dynamics of deformed 2D vortex Airy beams with arbitrary initial angles θ between the two wings. Because it is difficult to calculate the Fourier transform of deformed vortex Airy beams, our experimental setup is not similar to the Fourier transformation method that was used in our previous work[25]. Instead, we employ an off-axis hologram method like Ref. [27] to generate deformed 2D vortex Airy beams, and Fig. 5 shows our experimental setup.

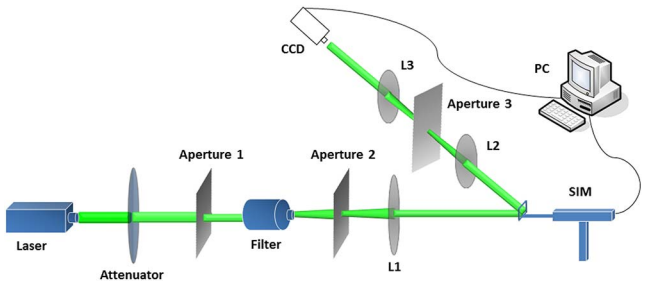

Fig. 5. (Color online) Experimental setup for the generation and propagation of deformed vortex Airy beams. PC: personal computer; L: lens.

A linearly polarized Gaussian beam with a wavelength of $\lambda = 532$ nm is launched onto a spatial light modulator (SLM) with the desired hologram, then a 4f system with a spatial filter turns the Gaussian beam into a deformed 2D vortex Airy beam. The generated deformed 2D vortex Airy beams are monitored by a CCD camera. Here, the hologram is manifested by computing the interference between a deformed vortex Airy wave and a plane wave.

The parameters adopted in our experiments are the same as those employed in the simulations shown in Figs. 1–4. The experimental results of the 2D vortex Airy beams for $m = 0, 1, 2$ with different initial wings angles are presented in Fig. 6, showing a good agreement with the results obtained from our previous analysis. When the holograms in Figs. 6(a4), 6(d4), and 6(g4) are used, viz., for $\theta = 60°$, as expected, the wing angle becomes larger along the propagation direction. In this case, the 2D Airy pattern cannot be preserved as it tends to evolve

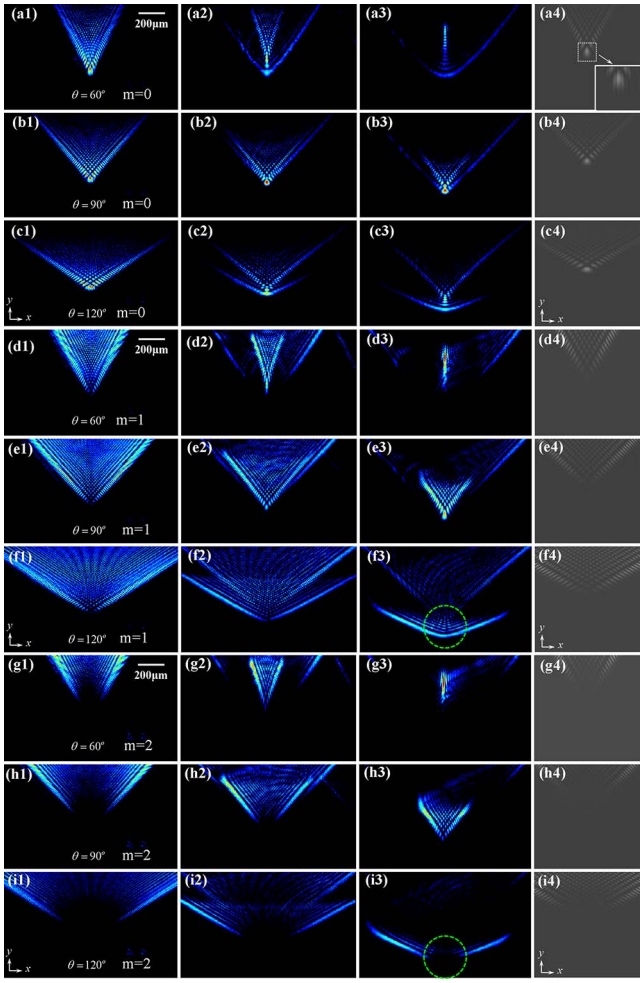

Fig. 6. (Color online) Experimental results showing the transverse intensity patterns captured at different propagation distances for deformed 2D vortex Airy beams with different initial angles between the two wings. From the 1st to the 3rd column are the beam profiles at $z = 0$ cm, $z = 4$ cm, and $z = 8$ cm, respectively, and the last column shows the corresponding holograms of the beams with different conditions.

into a 1D Airy-like shape to various degrees [Figs. 6(a), 6(d), and 6(g)]. On the other hand, when the holograms in Figs. 6(c4), 6(f4), and 6(i4) are used, the angle between the two wings becomes smaller during propagation [Figs. 6(c), 6(f), and 6(i)]. In addition, as the topological charge increases, more and more intensity falls on the 1D Airy-like pattern, in agreement with Figs. 1–3(c). For all of these cases, one can also see that the acceleration of the main lobe varies with respect to the angle θ between the two wings.

In addition, we can observe that, for a bigger topological charge, the peak intensity starts to reappear on the main lobe at a longer propagation distance [Figs. 6(d4)–6(i4)]. For example, in the middle of the intensity distributions in Fig. 6(f3) ($m = 1$) has yielded the peak intensity on its main lobe but the beam in Fig. 6(i3) ($m = 2$) still has no intensity to restore on the same transversal position [marked by the green dashed circles in Figs. 6(f3) and 6(i3)]. For the case of an acute angle in Figs. 6(a), 6(d), and 6(g), the influence of the topological charge m becomes larger, leading to a more evident shift of the peak intensity from the main lobe to the sub lobes. It is more difficult to form a 1D-Airy-like pattern since the intensity on the main lobe position is largely reduced by this factor. Meanwhile, from Fig. 6, we can also find that a left-hand deflection exists that rises with an increasing topological charge and an increasing initial wing angle. Therefore, all experimental results are in excellent agreement with theory.

In conclusion, we investigate the ballistic dynamics of 2D vortex Airy beams with arbitrary initial angles between two wings through the split-step beam propagation method and the analysis of the energy flow. Our results show that these beams always follow two parabolic trajectories: one trajectory describes the acceleration of the main lobe, while the other describes the acceleration of the other energy flow. Both accelerations can be controlled with ease by means of the initial wing angles and the topological charge of the vortex Airy beams. Seemingly due to a "hyperbolic umbilic" catastrophe, these beams tend to evolve into 1D or 2D Airy-like patterns to various degrees after a certain propagation distance. Furthermore, the whole profiles of beams no longer accelerate along only one direction. A left-hand deflection happens and increases with an increasing topological charge and an increasing initial wing angle. For a bigger topological charge and a smaller initial wing angle, the main lobe takes a longer distance to restore to the peak intensity. Thus, we can control the peak intensity at any desired location by changing the parameters such as the topological charge and initial wing angle. Here, it should be pointed out, the above experimental and theoretical analysis can be applied for more complicated cases with larger topological charges as well. Our results may be useful for designing and controlling dynamical Airy beams for various applications.

This work was supported by the National Natural Science Foundation of China (Nos. 11604058 and 61367004), the Guangxi Key Laboratory for Relativistic Astrophysics-Guangxi Natural Science Creative Team Funding (No. 2013GXNSFFA019001), and the Guangxi Natural Science Foundation (No. 2016GXNSFBA380244).

References

1. G. A. Siviloglou and D. N. Christodoulides, Opt. Lett. **32**, 979 (2007).
2. G. A. Siviloglou, J. Broky, A. Dogariu, and D. N. Christodoulides, Phys. Rev. Lett. **99**, 213901 (2007).
3. J. Broky, G. A. Siviloglou, A. Dogariu, and D. N. Christodoulides, Opt. Express **16**, 12880 (2008).
4. J. Baumgartl, M. Mazilu, and K. Dholakia, Nat. Photon. **2**, 675 (2008).
5. J. Zhao, I. D. Chremmos, D. Song, D. N. Christodoulides, N. K. Efremidis, and Z. Chen, Sci. Rep. **5**, 12086 (2015).
6. P. Polynkin, M. Kolesik, J. V. Moloney, G. A. Siviloglou, and D. N. Christodoulides, Science **324**, 229 (2009).
7. A. Chong, W. Renninger, D. N. Christodoulides, and F. W. Wise, Nat. Photonics **4**, 103 (2010).
8. M. Clerici, Y. Hu, P. Lassonde, C. Milián, A. Couairon, D. N. Christodoulides, Z. Chen, L. Razzari, F. Vidal, F. Légaré, D. Faccio, and R. Morandotti, Sci. Adv. **1**, e1400111 (2015).
9. A. Minovich, A. E. Klein, N. Janunts, T. Pertsch, D. N. Neshev, and Y. S. Kivshar, Phys. Rev. Lett. **107**, 116802 (2011).
10. P. Zhang, S. Wang, Y. Liu, X. Yin, C. Lu, Z. Chen, and X. Zhang, Opt. Lett. **36**, 3191 (2011).
11. L. Li, T. Li, S. M. Wang, C. Zhang, and S. N. Zhu, Phys. Rev. Lett. **107**, 126804 (2011).
12. Q. Zhang, C. Tan, C. Hang, and G. Huang, Chin. Opt. Lett. **13**, 082401 (2015).
13. N. Voloch-Bloch, Y. Lereah, Y. Lilach, A. Gover, and A. Arie, Nature **494**, 331 (2013).
14. S. Jia, J. C. Vaughan, and X. Zhuang, Nat. Photon. **8**, 302 (2014).
15. T. Vettenburg, H. I. C. Dalgarno, J. Nylk, C. Coll-Lladó, D. E. K. Ferrier, T. Čižmár, F. J. Gunn-Moore, and K. Dholakia, Nat. Methods **11**, 541 (2014).
16. Y. Liang, Y. Hu, D. Song, C. Lou, X. Zhang, Z. Chen, and J. Xu, Opt. Lett. **40**, 5686 (2015).
17. Y. Liang, Z. Ye, D. Song, C. Lou, X. Zhang, J. Xu, and Z. Chen, Opt. Express **21**, 1615 (2013).
18. H. Dai, Y. Liu, D. Luo, and X. Sun, Opt. Lett. **35**, 4075 (2010).
19. R. P. Chen and C. H. R. Ooi, Phys. Rev. A **84**, 043846 (2011).
20. X. Chu, Opt. Lett. **37**, 5202 (2012).
21. R. P. Chen, K. H. Chew, and S. L. He, Sci. Rep. **3**, 1406 (2012).
22. Y. Zhu, L. Zhang, and Y. Zhang, Chin. Opt. Lett. **14**, 042101 (2016).
23. W. Wen and X. Chu, J. Opt. Soc. Am. A **31**, 685 (2014).
24. J. Zhang, Z. Pang, L. Feng, T. Zhong, L. Wang, and D. Deng, Chin. Opt. Lett. **15**, 060501 (2017).
25. Y. Liang, Y. Hu, Z. Ye, D. Song, C. Lou, X. Zhang, J. Xu, R. Morandotti, and Z. Chen, J. Opt. Soc. Am. A **31**, 1468 (2014).
26. M. Berry and C. Upstill, "Catastrophe optics: Morphologies of caustics and their diffraction patterns," in *Progress in Optics*, E. Wolf, ed. (Elsevier, 1980), p. 257.
27. P. Zhang, J. Prakash, Z. Zhang, M. S. Mills, N. K. Efremidis, D. N. Christodoulides, and Z. Chen, Opt. Lett. **36**, 2883 (2011).